AN INTEGRATED, VERTICAL-DRIVE, IN-PLANE-SENSE MICROGYROSCOPE

Sunil A. Bhave, Joseph I. Seeger, Xuesong Jiang, Bernhard E. Boser, Roger T. Howe and John Yasaitis*

Berkeley Sensor & Actuator Center, 497 Cory Hall, University of California, Berkeley, CA 94720, USA
*Analog Devices Inc., 21 Osborn Street, Cambridge, MA 02139, USA

ABSTRACT

This paper describes the principle of operation and experimental results of a Y-axis ΣΔ force-feedback gyroscope. The gyroscope was fabricated in Analog Devices' monolithic Modular-MEMS process with 6μm thick structural polysilicon and 0.8μm CMOS. The sensor utilizes vertical (Z-axis) actuation of the proof mass to enable in-plane (X-axis) differential sensing of the Coriolis force. Two orthogonally-oriented gyroscopes form a dual-axis rate sensor. The gyroscope achieves 8º/sec/√Hz noise floor, for operation at ambient pressure.

INTRODUCTION

Micromachined, monolithic accelerometers and gyroscopes have gained popularity in the automotive industry for air-bag deployment and roll-over detection systems and in consumer electronics for platform stabilization in camcorders and video-game headsets. These sensors need to operate at atmospheric pressure (hermetic packaging) with a 5V power supply to be cost-effective in the consumer market. Previous work at Berkeley has demonstrated a 3-axis accelerometer [1] and a Z-axis rate gyroscope that operates in air [2]. This paper presents an X/Y-axis rate gyroscope that complements these sensors and completes the 6 degree-of-freedom inertial measurement unit (IMU). A low-cost, monolithic IMU would increase the application space to active suspension and traction control systems for automobiles and can be used as a GPS-assistance unit in black-out areas.

Previous designs of lateral (Y-axis) rate gyroscopes can be classified into two categories:

- Rotor: Drive about Z-axis; rotation input Ω_Y generates Coriolis torque about X-axis [3,4]
- Plate: Drive along X-axis; rotation input Ω_Y generates Coriolis force along Z-axis [5,6]

Both approaches drive the proof-mass into oscillation parallel to the substrate and sense Coriolis force out-of-plane. Problems with out-of-plane displacement sensing include difficulty in implementing differential sense pick-off due to the parasitic capacitances associated with the electrode layer, and inability to implement force-feedback since there are no electrodes above the structural layer to apply a feedback force in the upward direction. In addition, these gyroscopes have to be vacuum encapsulated because they experience squeeze-film damping in the vertical sensing direction. Recently a lateral-axis gyroscope with out-of-plane drive and in-plane Coriolis sensing was presented [7]. However, due to fabrication technology constraints, the drive and sense springs of the gyroscope are parallel, resulting in mode-coupling between the drive-mass and the sense-frame.

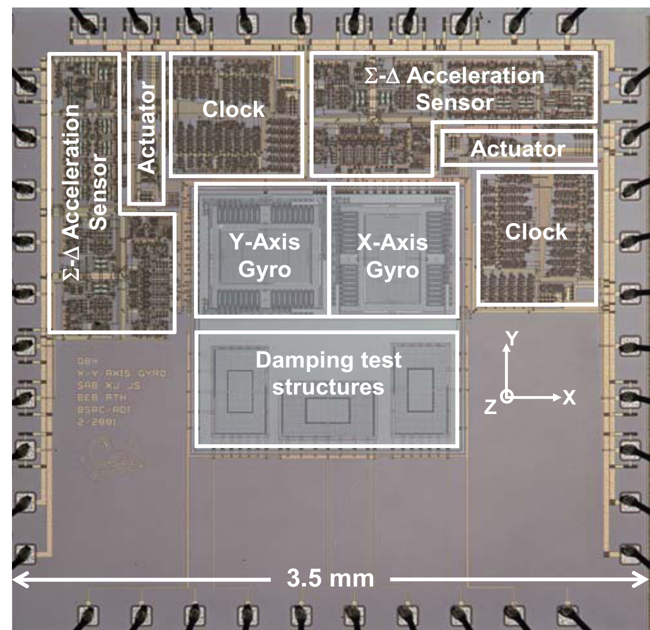

Figure 1: *Photograph of dual-axis rate sensor.*

Our design incorporates a decoupled frame suspension [6] and in-plane Coriolis sensing to implement a decoupled, vertical-drive Y-axis rate gyroscope. Both, the Z-axis gyroscope [2] and the vertically-driven Y-axis gyroscope have a sense frame that detects Coriolis acceleration along the X-axis. Therefore, we can divide the IMU into three modular building blocks: a Y-axis (lateral) oscillator, a Z-axis (vertical) oscillator, and a ΣΔ force-feedback X-axis (lateral) accelerometer. This paper focuses on the Z-axis oscillator and the suspension design to decouple the oscillator from the Coriolis sensing frame.

DESIGN SUMMARY

The photograph of the X&Y-axis rate gyroscope is shown in Figure 1. The sensor was fabricated by Analog Devices in the Modular-MEMS process with 6μm thick mechanical polysilicon layer and 5V, 0.8μm CMOS technology [8].

0-7803-7731-1/03/$17.00 ©2003 IEEE

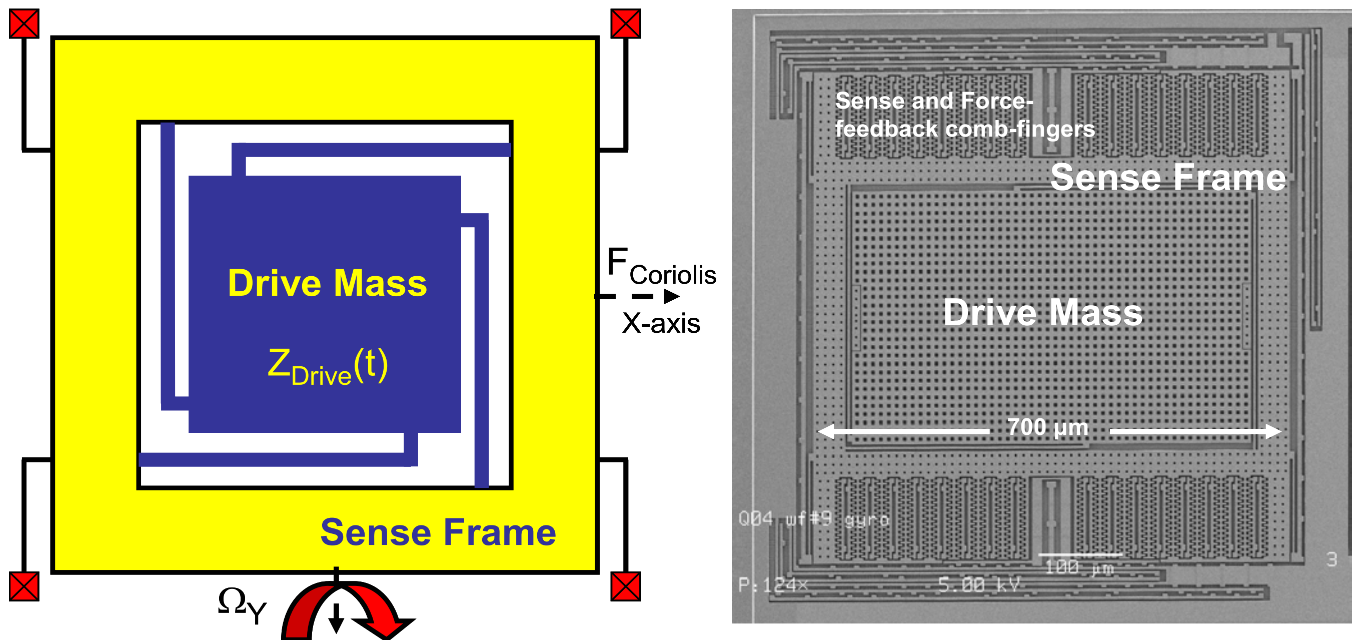

Figure 2: *Schematic and SEM of the Y-axis rate gyroscope. The SEM shows the differential comb-fingers for Coriolis sensing and force-feedback. The drive-mass has long, wide springs and the sense-frame has short, thin suspension springs.*

A schematic diagram and SEM of the frame suspension of the Y-axis gyroscope is shown in Figure 2. The inner drive-mass is actuated along the Z-axis (out of the plane of the chip) using a parallel-plate electrode underneath the structure. Rotation about the Y-axis generates Coriolis acceleration along the X-axis. Lateral displacement of the sense-frame, due to Coriolis acceleration, is detected by a ΣΔ capacitive interface circuit. In contrast to traditional Y-axis gyroscopes, the parallel-plate capacitive transducer is used for vertical actuation, and differential lateral comb-fingers are used for in-plane sensing and force-feedback. The resonant frequency and quality factor at ambient pressure, are approximately 14.5 kHz and 2 for the drive-mass and 16.2 kHz and 20 for the sense-frame. The drive-mass area is 300µm × 500µm, while the total sensor area is approximately $(700\mu m)^2$.

The drive electronics consist of an off-chip oscillator and on-chip Schmidt trigger to ensure that the drive-mass experiences 5V square wave excitation at the oscillator frequency. The proof-mass is driven approximately ±0.15µm along the Z-axis at the sense-frame resonant frequency, to take advantage of the sense quality factor. The sense electronics implement a ΣΔ feedback loop and are explained in detail in [9].

SUSPENSION DESIGN

The vertical-drive and in-plane sense modes of the Y-axis gyroscope are illustrated in Figure 3. The asymmetric drive-mass suspension ensures that it is axially and torsionally stiff about the X- and Y-axes [6]. The next low frequency mode after the vertical 'bouncing' mode is the diagonal tipping-mode. This mode is 5 kHz higher than the vertical-drive mode and therefore well isolated from the operating frequency.

For a Y-axis frame gyroscope the suspension spring of the sense-frame has to be compliant along the X-axis and stiff along the Z-axis, to ensure that the sense-frame does not 'bounce' during vertical actuation of the drive-mass. The Modular-MEMS process provides flexibility to design cantilevers with 5:1 aspect ratios. This provides us the flexibility to design cantilever suspension springs with out-

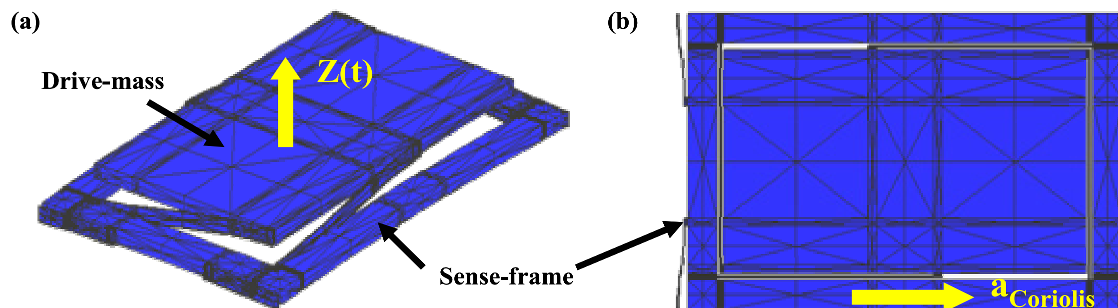

Figure 3: *Decoupled (a) vertical drive mode and (b) in-plane sense mode.*

of-plane to in-plane stiffness ratio of up to 25:1. We have designed the sense-frame suspension with compliance along the X-axis (for mode-matching), and 25× stiffness, relative to the drive-mass, in the Z-direction (for mode-decoupling). Such design-space flexibility is not available in a generic 1:1 aspect ratio surface micromachining technology. In addition, zero residual stress in the structural polysilicon layer of Modular-MEMS process, allows us to design simple suspensions without any stress relief features.

VERTICAL ACTUATOR

In a vibratory rate gyroscope, the Coriolis force on the sense frame is $F_{Coriolis,X-axis} = 2 \times (m_{Drive} \times z \times \omega_Z) \times \Omega_{Y-input}$. For operation at atmospheric pressure, we do not expect large vertical-drive amplitude and hence maximize the Z-axis momentum vector by increasing the mass and resonant frequency of the vertical-drive mode.

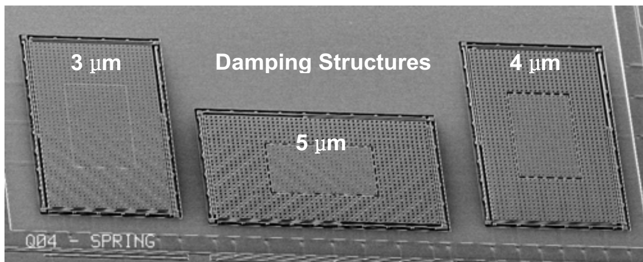

Figure 4: *Vertical oscillator structure array with 3,4 and 5µm etch-holes. All structures have identical mass, spring constant and actuation area.*

The drive-mass is actuated in the vertical direction by using a parallel plate actuator defined in the electrode layer, 1.6µm below the structure layer. The mass is perforated with 5µm × 5µm etch-holes, spaced by 10µm. These large etch-holes are to ensure that we can get relatively large motion of the drive-mass, even in the presence of large-amplitude squeeze-film damping. A set of damping test structures with different sized etch-holes (Figure 4), but with identical mass, actuation area and resonant frequency, were designed to characterize squeeze-film damping in the vertical direction.

Figure 5 summarizes the results of this experiment. All measurements were made using a 3D interferometer system [10], with a 5V sinusoidal signal applied to the drive electrode. We observe that the proof-mass with 3µm etch-holes is over-damped, while the 5µm etch-hole mass has a quality factor of 2 at 14.5 kHz. The vertical amplitude of ±0.18µm at resonance was 4× lower than that predicted using known squeeze-film models [11]. Electrostatic spring-softening due to the parallel-plate capacitive drive is evident in the 5µm etch-hole mass. Future designs will incorporate 6µm or even larger etch-holes; however structural rigidity of the drive-mass with such large perforations will have to be reconsidered.

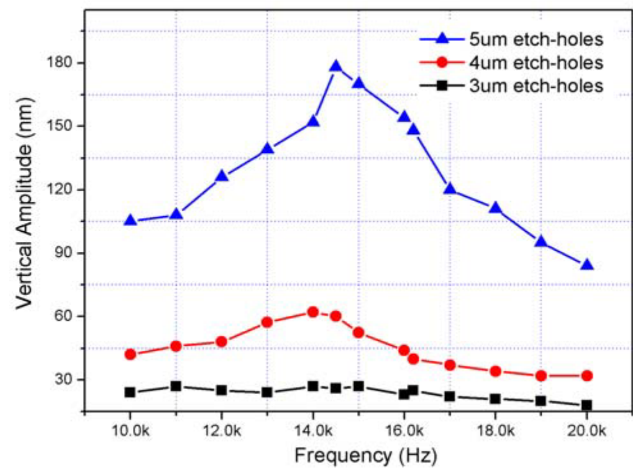

Figure 5: *Vertical amplitude of damping test structures.*

EXPERIMENTAL RESULTS

The drive-mass was excited at 16.2 kHz (sense resonance) to take advantage of the noise shaping of the X-axis accelerometer sensor (Figure 6). The interferometer measured 150 nm vertical amplitude motion at ambient pressure.

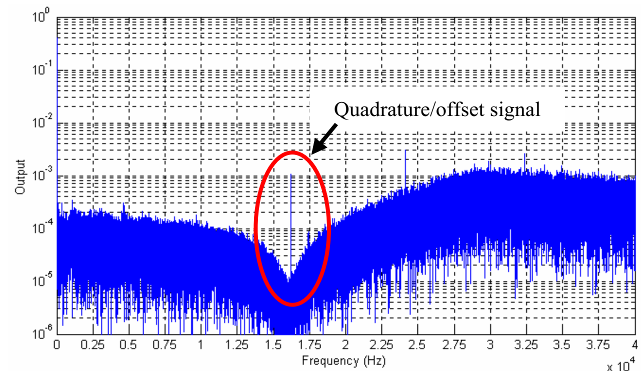

Figure 6: *Raw measured bit-stream output spectrum shows ΣΔ noise shaping.*

The gyroscope was tested on a rate table and the 1-bit output bit-stream of the ΣΔ modulator was processed using Matlab. Figure 7 shows the output spectrum of the gyroscope in response to a 94°/sec and 2Hz sinusoidal rotation. The vertical motion of the proof-mass is reduced by squeeze-film damping, limiting the gyroscope performance to 8°/sec/√Hz noise floor in air. The ΣΔ capacitive interface has been characterized on a shaker table to evaluate its acceleration sensitivity and displacement resolution. The noise floor of the X-axis accelerometer is 2mg/√Hz at low frequencies and 115µg/√Hz at the sense resonance.

An underexposure of the structural polysilicon mask has been identified as the main cause of performance degradation of the gyroscope. The underexposure caused a 7% increase in the widths of the drive and sense suspension springs and reduced drive-mass etch-hole sizes to $(4.7\mu m)^2$.

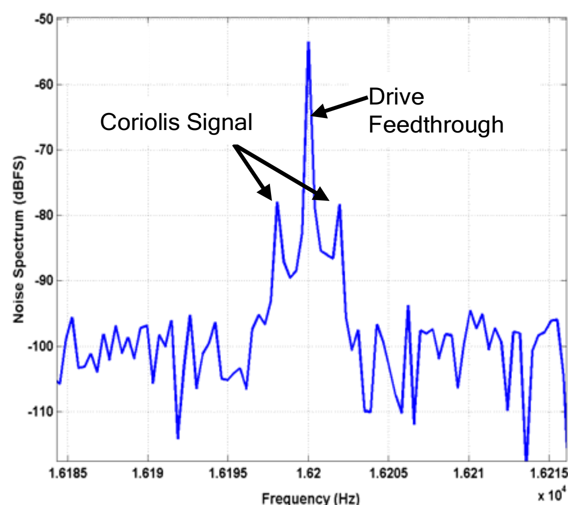

Figure 7: *Gyroscope output response to a 94°/sec (0-peak) 2Hz sinusoidal rate signal.*

This causes the drive-mode resonant frequency to be lower than the sense-mode resonant frequency. It also considerably increased the squeeze-film damping in the vertical direction, thereby by reducing the drive quality factor to approximately two.

In addition, a pair of shielding electrodes was erroneously placed next to the drive-mass. Although we attempted to minimize damping in the X-direction by using lateral comb-fingers on the sense-frame, the gyroscope experiences squeeze-film damping between the drive-mass (which moves along with the sense-frame) and the shield electrodes, thereby reducing the sense quality factor to ~20. Overall we estimate that the underexposure during lithography and erroneous shield design resulted in approximately 5× degradation in the sensitivity of the gyroscope. Table 1 summarizes the performance of the rate sensor.

Table 1: *Performance summary of the Y-axis gyroscope.*

Mass	1.6μgm (drive) 2.8μgm (sense)
Resonant frequency	14.5 kHz (drive) 16.2 kHz (sense)
Quality factor	2 (drive) 20 (sense)
Noise floor	8°/sec/√Hz

CONCLUSIONS

We have demonstrated a vertical-drive, in-plane-sense microgyroscope, which operates at atmospheric pressure, with a 1-bit output from the ΣΔ capacitive interface. Large amplitude squeeze-film damping in the vertical direction has been characterized. We have determined that >6μm etch-holes are necessary to achieve substantial drive-mass vibration amplitude. Imperfections in lithography and gyroscope design lead to an overall noise floor of 8°/sec/√Hz at atmospheric pressure.

ACKNOWLEDGMENTS

This research was funded by DARPA under agreement F30602-97-2-0266. We would like to thank Thomas Chen of Analog Devices for the SEMs and Rishi Kant at BSAC for assistance with the 3D interferometer.

REFERENCES

[1] M. A. Lemkin, M. A. Ortiz, N. Wongkomet, B. E. Boser, J. H. Smith, "A 3-axis surface micromachined ΣΔ accelerometer," *ISSCC Dig. Tech. Papers*, San Francisco, CA, February (1997), pp. 202–203.

[2] J. I. Seeger, X. Jiang, M. Kraft, B. E. Boser, "Sense Finger Dynamics in a ΣΔ Force-Feedback Gyroscope," *Solid State Sensor and Actuator Workshop*, Hilton Head Island, SC, June (2000), pp. 296-299.

[3] T. Juneau, A. P. Pisano, "Micromachined Dual Input Axis Angular Rate Sensor," *Solid State Sensor and Actuator Workshop*, Hilton Head Island, SC, June (1996), pp. 299-302.

[4] K. Funk, H. Emmerich, A. Schilp, M. Offenberg, R. Neul, F. Larmer, "A Surface Micromachined Silicon Gyroscope using Thick Polysilicon Layer," *MEMS'99*, Orlando, FL, January (1999), pp. 57-60.

[5] J. Bernstein, S. Cho, A.T. King, A. Kourepenis, P. Maciel, M. Weinberg, "A Micromachined Comb-Drive Tuning Fork Rate Gyroscope," *MEMS'93*, Fort Lauderdale, FL, January (1993), pp. 143-148.

[6] Y. Mochida, M. Tamura, K. Ohwada, "A Micromachined Vibrating Rate Gyroscope with Independent Beams for the Drive and Detection Modes," *MEMS'99*, Orlando, FL, January (1999), pp. 618-623.

[7] H. Xie, G. Fedder, "A CMOS-MEMS Lateral-axis Gyroscope," *MEMS'01*, Interlaken, Switzerland, January (2001), pp. 162-165.

[8] J. Yasaitis *et al*, "A Modular Process for Integrating Thick Polysilicon MEMS Devices with Sub-Micron CMOS," *Proceedings of SPIE vol. 4979*, San Jose, CA, January (2003), pp. 145-154.

[9] X. Jiang, S.A. Bhave, J.I. Seeger, R.T. Howe, B.E. Boser, J. Yasaitis, "ΣΔ Capacitive Interface for a Vertically-Driven X&Y-Axis Rate Gyroscope," *28th European Solid-State Circuits Conference*, Florence, Italy, September (2002), pp. 639-642.

[10] C. Rembe, L. Muller, R. S. Muller, R. T. Howe, "Full Three-Dimensional Motion Characterization of a Gimbaled Electrostatic Microactuator," *2001 IEEE International Reliability Physics Symposium*, Orlando, FL, April (2001), pp. 91-98.

[11] E. S. Kim, Y. H. Cho, M. U. Kim, "Effect of Holes and Edges on the Squeeze Film Damping of Perforated Micromechanical Structures," *MEMS'99*, Orlando, FL, January (1999), pp. 296-301.